# Autophagy is required for cell survival under L-asparaginase－induced metabolic stress in acute lymphoblastic leukemia cells

# Autophagy is required for cell survival under L-asparaginase–induced metabolic stress in acute lymphoblastic leukemia cells

Hiroyoshi Takahashi[1,2,3], Jun Inoue[1,3], Kimiyoshi Sakaguchi[2], Masatoshi Takagi[4], Shuki Mizutani[4], Johji Inazawa[1,3]

**Author's affiliations:** [1]Department of Molecular Cytogenetics, Medical Research Institute, Tokyo Medical and Dental University, Tokyo, Japan; [2]Department of Pediatrics, Hamamatsu University School of Medicine, Shizuoka, Japan; [3]Bioresource Research Center, Tokyo Medical and Dental University, Tokyo, Japan; [4]Department of Pediatrics and Developmental Biology, Tokyo Medical and Dental University, Tokyo, Japan

**Correspondence:** Jun Inoue and Johji Inazawa, Department of Molecular Cytogenetics, Medical Research Institute, Tokyo Medical and Dental University. 1-5-45 Yushima, Bunkyo-ku, Tokyo 113-8510, Japan; e-mail: jun.cgen@mri.tmd.ac.jp (Jun Inoue), johinaz.cgen@mri.tmd.ac.jp (Johji Inazawa); TEL: +81-3-5803-5820, FAX: +81-3-5803-0244.

**Running title:** Role of autophagy in L-asparaginase–treated ALL cells

**Keywords:** autophagy, acute lymphoblastic leukemia, L-asparaginase; reactive oxygen species, p53

**Conflict of interest:** The authors declare no conflict of interest.

**Other notes:** A total of 3,854 words.

**ABSTRACT**

L-asparaginase has been used for more than three decades in acute lymphoblastic leukemia (ALL) patients and remains an essential drug in the treatment of ALL. Poor response to L-asparaginase is associated with increased risk of therapeutic failure in ALL. However, both the metabolic perturbation and molecular context of L-asparaginase–treated ALL cells has not been fully elucidated. Here we identify that treatment with L-asparaginase results in metabolic shutdown via the reduction of both glycolysis and oxidative phosphorylation, accompanied by mitochondrial damage and activation of autophagy. The autophagy is involved in reducing reactive oxygen species (ROS) level by eliminating injured mitochondria. Inhibition of autophagy enhances L-asparaginase-induced cytotoxicity and overcomes the acquired resistance to L-asparaginase in ALL cells. The ROS-p53 positive feedback loop is an essential mechanism of this synergistic cytotoxicity. Thus, our findings provide the rationale for the future development of combined treatment of L-asparaginase and anti-autophagy drug in ALL patients.

## INTRODUCTION

Acute lymphoblastic leukemia (ALL) is the most common type of childhood cancer[1]. Although treatment outcomes have been remarkably improved by the development of effective therapies and well-designed protocols, approximately 20% of pediatric patients develop resistance to therapy and eventually relapse, often leading to death[1, 2]. L-asparaginase (L-asp), one of the most important drugs used for childhood ALL therapy, is an enzyme that catalyzes the hydrolysis of asparagine (Asn) or glutamine (Gln) to aspartic acid (Asp) or glutamic acid (Glu), respectively[3]. Poor response to L-asp is associated with increased risk of relapse and therapeutic failure[4, 5]. It has been proposed that the sensitivity of ALL to L-asp is due to low or absent expression of asparagine synthetase (ASNS)[6-8]. However, genome-wide expression profiling of ALL patient samples showed conflicting results[9-11], and basal ASNS expression was shown to have no clinical significance in ALL patients[12]. Thus, despite long-standing experience with L-asp therapy, both the metabolic perturbation and molecular context of L-asp–treated ALL cells remains to be fully elucidated.

One of the major cellular responses to amino acid depletion is the induction of autophagy. Autophagy is a degradation process of proteins and organelles, which can provide metabolic intermediates such as amino acids, and can also reduce reactive oxygen species (ROS)-mediated oxidative stress by eliminating damaged mitochondria[13]. Some anticancer drugs can induce cytoprotective autophagy[14], and several clinical trials using combined treatment of existing anticancer drugs and the lysosomal inhibitor chloroquine (CQ) are currently ongoing[15]. Treatment with L-asp can also induce cytoprotective autophagy in human cancers[16-18]. However, the biological significance of L-asp–induced autophagy or the effect of autophagy inhibition in L-asp–treated cells remains largely unknown. In this study, we sought to reveal how L-asp affects cellular processes in ALL cells, and to elucidate the implication of L-asp–induced autophagy in hopes of obtaining insight into alternative strategies for ALL therapy.

## RESULTS

*L-asparaginase treatment induces metabolic shutdown and mitochondrial injury in ALL cells*

We first confirmed that intracellular Asn and Gln were immediately depleted in REH cells during L-asp treatment (Figure 1a). To understand the physiological effect of L-asp treatment, we next performed the gene expression array of L-asp-treated REH cells, accompanied by gene ontology (GO) analysis using Database for Annotation, Visualization, and Integrated Discovery (DAVID)[19] and gene set enrichment analysis (GSEA)[20]. The expression levels of genes associated with several cellular metabolic pathways, including glycolysis, tricarboxylic acid (TCA) cycle, and oxidative phosphorylation (OXPHOS), were significantly lower in L-asp–treated REH cells than in untreated cells (Figures 1b and c and Supplementary Table S2). Decreased expression levels of these metabolism-related genes were also confirmed in two ALL cell lines, REH and 697, by qRT-PCR (Figure 1d and Supplementary Figure S1). These findings were consistent with the decrease of intracellular ATP level (Figure 1a) and the result from the energy metabolism analysis using the XF24 extracellular flux analyzer; basal levels of both the oxygen consumption rate (OCR) for OXPHOS in the mitochondria and the extracellular acidification rate (ECAR) for glycolysis were remarkably lower in L-asp–treated cells than in untreated cells (Figure 1e), suggesting that L-asp treatment effectively induces metabolic shutdown in ALL cells. In a mitochondrial stress test, treatment with oligomycin, an Fo-ATPase inhibitor of Complex V, clearly reduced mitochondrial respiration in L-asp–treated and untreated cells. However, spare respiratory capacity (defined as the quantitative difference between maximal OCR after addition of mitochondrial oxidative phosphorylation uncoupler FCCP and the initial basal OCR) in L-asp–treated cells was significantly lower than in untreated cells (Figure 1f). These data suggested that L-asp treatment induces metabolic shutdown accompanied by reduction of both glycolysis and OXPHOS, and mitochondrial function is heavily impaired in L-asp–treated cells.

*L-asparaginase–induced autophagy is involved in reducing reactive oxygen species level by eliminating injured mitochondria*

To investigate whether L-asp treatment induced autophagy in ALL cells, we next evaluated autophagy flux in ALL cells by detection of LC3B form-II (LC3B-II), an autophagosome marker[21]. By western blotting, LC3B-

II levels were observed to be increased by L-asp treatment, and this increase was significantly enhanced by inhibiting autophagosome turnover via the addition of a lysosomal inhibitor, CQ or bafilomycin A1 (Baf) (Figure 2a and Supplementary Figure S2A). In immunofluorescence analysis, LC3B-positive autophagic puncta were observed in L-asp–treated REH cells, and the number of these puncta was remarkably increased by the addition of CQ (Figure 2b). Moreover, electron microscopic analysis revealed that both the number and area of autophagic vacuoles per cell were significantly increased in L-asp–treated REH cells, and these increases were clearly enhanced by addition of CQ (Figure 2c). These findings suggest that L-asp treatment can induce autophagy in ALL cells.

Furthermore, intracellular amino acids profiles revealed that both Asn and Gln levels rapidly decreased after L-asp treatment, however the rate of decrease of these amino acids in the L-asp–treated cells did not significantly differ between cells treated with or without CQ (Supplementary Figure S2B), suggesting that autophagy might not contribute to supply a detectable amount of these amino acids. In contrast, the feature of mitochondrial injury such as the decreased mitochondrial membrane potential ($\Psi_m$) and the increase of both intracellular and mitochondrial ROS levels were remarkably enhanced autophagy-inhibited REH cells during L-asp treatment (Figures 2d and e and Supplementary Figures S2C–E). In addition, L-asp treatment significantly induced a decrease of amount mitochondrial DNA and mitochondrial mass (Supplementary Figures S2F and G). Taken together, these data suggested that L-asp–induced autophagy functions predominantly in mitochondrial quality control rather than in recycling intracellular amino acids.

*Autophagy inhibition enhances the cytotoxicity of L-asparaginase treatment*

We then examined the effect of autophagy inhibition on L-asp–induced cytotoxicity in ALL cell lines. When autophagic degradation was pharmacologically inhibited by treatment with CQ simultaneously with L-asp treatment, the number of dead cells remarkably increased compared to L-asp alone (Figure 3a). Apoptotic cells, indicated by increased levels of cleaved caspase-3 and cleaved PARP, were clearly detected with combined treatment of L-asp and CQ (Figure 3b). For cell cycle analysis, the treatment with L-asp alone induced cell cycle arrest at the G1 phase, consistent with a previous report[22], and the combined treatment with CQ and L-asp significantly increased the sub-G1 population (Supplementary Figure 3A). Concurrent treatment

with the caspase inhibitor zVAD-fmk inhibited the induction of cell death by combined treatment of L-asp and CQ (Supplementary Figure S3B). Treatment of ALL cells with L-asp showed significantly synergistic anti-leukemic effects in combination with autophagy inhibition using CQ (combination index at the IC50 = 0.515 in REH cells and 0.686 in 697 cells) (Supplementary Figure S3C). We next investigated the effect of prolonged treatment exposure with L-asp. Almost all cells treated with the combination of L-asp and CQ died after 6–9 days, whereas cells treated with L-asp or CQ alone remained viable and continued to slowly proliferate during treatment (Figure 3c). This combined effect was also observed when autophagy was inhibited by siRNA-mediated knockdown of the essential autophagy genes including *ATG7*, *ATG5,* and *BECN1* (*Beclin1*) (Figure 3d and Supplementary Figure 3D). Furthermore, we examined the inhibitory effect of autophagy process at the early stage by treatment with 3MA or at the late stage by treatment with ALLN, a cathepsin inhibitor. As the result, the clear synergistic effect was shown in both combined treatment, suggesting that blocking autophagy flux can enhance L-asp–induced toxicity in ALL cells. (Supplementary Figures S3E and F). Particularly, the synergistic effect by CQ treatment was not shown in the cells whose autophagy was clearly inhibited by treatment with 3MA (Supplementary Figure S3G), suggesting that CQ-mediated sensitization is dependent on inhibiting autophagy.

To test whether autophagy inhibition can overcome the resistance to L-asp treatment, we generated the acquired resistant cells from 697 cells by prolonged exposure to L-asp (parental 697 cells; IC50 = 0.74 and 697-R cells, a resistant 697 cells; IC50 = 2.4) (Figure 3e). Combined treatment of L-asp and CQ induced significant cell death, including in 697-R cells (Figure 3f). Importantly, LC3B-II levels were increased in 697-R cells more than in parental 697 cells by L-asp treatment, and this increase was significantly enhanced by CQ treatment, suggesting the activity of L-asp–induced autophagy in 697-R cells was higher than that of the parental 697 cells (Figure 3g). Thus, these finding suggest that autophagy inhibition may be a useful strategy to overcome L-asp resistance.

*Combination treatment of L-asparaginase and chloroquine suppresses leukemia growth in vivo*

To examined the therapeutic potential of the combined treatment using an *in vivo* ALL xenograft model, REH cells stably expressing luciferase (REH-Luc2) were injected into the tail vein of NOD/SCID mice.

Quantification of leukemia-associated bioluminescence at seven days after transplantation demonstrated no significant differences among the four treatment groups (Figure 4a). The mice then received daily intraperitoneal injections of PBS, 6 U/g L-asp, 50 mg/kg CQ, or both L-asp and CQ. Asn levels in the plasma of mice treated with L-asp were completely depleted (Figure 4b). A decrease in leukemia burden and increase in outcome improvement were observed in mice administered L-asp and CQ combined treatment, compared with mice treated with L-asp or CQ alone (Figures 4c and d, and Supplementary Figure S4A). This therapeutic effect by combined treatment with L-asp and CQ was also observed in other xenograft model using 697-Luc2 cells (Supplementary Figures S4B and C). Since hepatomegaly is caused by infiltration of leukemia cells, the liver weight of mice with leukemia is used as the indicator of objective response to anti-leukemic agents on some occasions[23, 24]. Mice treated with L-asp or CQ alone were found to have significantly decrease body weight and increase liver weight compared with mice administered L-asp and CQ combined treatment (Figures 4e and f), which indicate a remarkable anti-leukemic response. In addition, we could not find any signs of the treatment-related complication including hemorrhage or infarction in the sacrificed mice. Importantly, LC3B-positive puncta were observed to be accumulated in ALL cells that remained within the bone marrow, peripheral blood, and central nervous system of the mice receiving combined treatment, indicating the therapeutically sufficient autophagy inhibition (Supplementary Figure S5). These findings strongly suggested that combined treatment with L-asp and CQ may be therapeutically useful for ALL.

*The ROS-p53 positive feedback loop is an essential mechanism of the combined treatment of L-asparaginase and chloroquine*

We attempt to determine the molecular mechanism underlying the synergistic effect of L-asp–induced cytotoxicity and autophagy inhibition. Although the apoptosis pathway via the ATF4-CHOP axis is known to be involved in L-asp–induced cytotoxicity[25], this pathway was not significantly activated in cells treated with the combination of L-asp and CQ, compared with the cells treated with L-asp alone (Supplementary Figure S6), suggesting that other mechanism may contribute to the induction of cell death by combined treatment with L-asp and CQ. We then focused on the production of ROS as a possible mechanism, because ROS levels were remarkably increased during combined treatment (Figure 2e). ROS scavenger NAC rescued the induction of

cell death by combined treatment with L-asp and CQ (Figure 5a and Supplementary Figure S7A), indicating that excessive ROS accumulation is critical for the induction of cytotoxicity by the combined treatment. Severe ROS accumulation leads to irreparable DNA damage, which may induce the ROS-DNA damage-p53 positive feedback loop[26]. The protein expression levels of p53 and PUMA were remarkably increased, and was accompanied by DNA damage indicated by an increased level of γH2AX, in cells treated with the combination of L-asp and CQ compared with cells treated with L-asp alone in both REH and 697 cells with TP53 wild-type (Figure 5b and Supplementary Figure S7B). The inhibition of ROS production by treatment with NAC led to the reduction of both DNA damage and p53 expression (Figure 5c and Supplementary Figure S7C). *TP53* knockdown resulted in the reduction of ROS and DNA damage in cells treated with the combination of L-asp and CQ (Figures 5d and e and Supplementary Figures S7D and E). TP53 is known to play multiple roles in the regulation of autophagy[27]. In western blot analysis, knockdown of *TP53* did not exert a sever influence on L-asp–induced autophagy (Supplementary Figures S7F). Importantly, when *TP53* expression was inhibited by differential two knockdown system using shRNA or siRNA, the synergistic cytotoxic effect of L-asp and CQ combined treatment was abrogated (Figure 5f and Supplementary Figures S7G and H). Activated p53 transcriptionally up-regulated the pro-oxidant genes, including *PUMA*, *TP53I3*, *SCO2*, and down-regulated the anti-oxidant gene *HK2* (Supplementary Figure S7I). Additionally, in overall survival analysis of mice transplanted with *TP53*-knockdown or control ALL cells treated with L-asp and CQ combination, poor outcome was observed in mice transplanted with *TP53*-knockdown ALL cells (sh-p53), similar to those receiving no treatment (Figure 5g). We finally examined the functional role of p53 on the synergistic effect of L-asp and CQ combination treatment in seven primary ALL samples, including six cases with wild-type *TP53* and one case with mutant *TP53* (R248Q). These samples were derived from five newly diagnosed patients and two relapsed patients. Clinical features of these patients are shown in supplementary Table 3. As expected, the synergistic effect of L-asp and CQ was observed in ALL cells derived from the six wild-type *TP53* samples, but not in ALL cells from the mutant *TP53* sample (Figure 5h). In addition, adenovirus-mediated expression of exogenous *TP53* into *TP53*-mutated ALL cells from No.7 patient or *TP53*-mutated ALL cell lines, Jurkat and CCRF-CEM, induced the synergistic effect by combined treatment with L-asp and CQ (Figure 5i and

supplementary Figure S7J). These findings strongly suggest that p53 function is essential for this synergistic effect.

## Discussion

In the present study, we clarified the physiological effect of L-asp and the biological significance of L-asp–induced autophagy, and additionally demonstrated the therapeutic effectiveness of autophagy inhibition by CQ in combination with L-asp treatment in ALL cells. The treatment with L-asp results in metabolic shutdown via the reduction of both glycolysis and oxidative phosphorylation, accompanied by mitochondrial injury and ROS production. Importantly, we demonstrated that the inhibition of autophagy using CQ enhances L-asp–induced cytotoxicity and overcomes the acquired resistance to L-asp in ALL cells via ROS-p53 positive feedback loop as an essential mechanism of this synergistic cytotoxicity.

Several studies have suggested that autophagy may act as a cytoprotective mechanism in tumor cells and that therapy-induced cell death can be enhanced upon autophagy inhibition[18, 28-30]. It has been reported that cytoprotective autophagy was induced by treatment with L-asp and autophagy inhibition enhanced L-asp–induced cytotoxicity in K562 cells, a chronic myeloblastic leukemia cell line. However, the functional role of L-asp–induced autophagy has not been clarified. While it has been believed that L-asp–induced autophagy contributes to the supply of amino acids including Asn and Gln[16-18, 31], our data in the current study suggest that L-asp–induced autophagy predominantly has a function as elimination of damaged mitochondrial rather than supply of intracellular amino acids by recycling. In treatment of patients with ALL, L-asp is used in combination with vincristine and prednisone[2]. Prednisone is reported to induce autophagy, which is required for cell death[32-34]. Thus, the modulation of autophagy by CQ needs to consider autophagic effect on combined drugs other than L-asp in the clinical setting of ALL.

We demonstrated in an ALL xenograft model that autophagy inhibition using CQ with L-asp treatment is therapeutically effective. Notably, the effect of L-asp and CQ combined treatment could be observed in ALL cells that remained within the bone marrow and central nervous system, suggesting the potency of autophagy inhibition with CQ in combination with L-asp treatment in intractable ALLs. In addition to clinical trials utilizing the inhibition of autophagy by CQ for treatment of solid tumors in adults, CQ is clinically used as an FDA-approved drug for treatment of pediatric patients with several diseases, such as malaria and interstitial lung disease[35, 36]. However, CQ may cause severe side effects, including irreversible retinal toxicity[36]. Moreover, CQ is not a specific autophagy inhibitor, but also modulates various additional

signal transduction pathways[37]. Therefore, development of therapeutic agents that can specifically inhibit the autophagy pathway is required for the clinical use.

We showed that functional p53 is needed for the synergistically cytotoxic effect of L-asp and CQ combined treatment in ALL cells. While autophagy was shown to be required for the development of Ras-driven pancreatic tumors in a previous study, autophagy inhibition by CQ promoted tumorigenesis in developing tumors lacking p53[38]. Another study reported that p53 plays an important role in the combined effect of temozolomide and CQ in glioblastoma[39]. Thus, these previous reports together with the present results suggest that functional p53 plays an essential role in autophagy inhibition-mediated cytotoxicity. Because mutations of the *TP53* gene are observed in approximately 6–8% of pediatric ALL patients[40], the majority of pediatric patients may benefit from the combined effect of autophagy inhibition and L-asp treatment.

In summary, we reported molecular evidence supporting the development of a novel therapeutic strategy of combined L-asp and autophagy inhibition for ALL. It will be important for ALL patients to evaluate the autophagy flux before, after, or during L-asparaginase treatment. Further validation of this strategy, together with determination of p53 status, in a large cohort of patients are warranted to effectively evaluate its impact on the treatment of ALL.

## MATERIALS AND METHODS

*Cell culture and reagents*

*TP53*-intact ALL cell lines, REH and 697, or *TP53*-mutated ALL cell lines, CCRF-CEM and Jurkat, were maintained in RPMI1640 medium supplemented with 10% fetal bovine serum, penicillin and streptomycin. Culture medium was changed 24 h before treatment for each experiment. REH (CRL-8286), CCRF-CEM (CRL-8436), and Jurkat (TIB-152) are commercially available from the American Type Culture Collection, and 697 is available from DSMZ (German, catalog code ACC 42). LEUNASE was used for L-asparaginase treatment, purchased from Kyowa Hakko Kirin Co.. Chloroquine diphosphate, Bafilomycin A1, and N-acetyl-L-cysteine (NAC) were purchased from Sigma-Aldrich Co..

*Patients*

Bone marrow with more than 90% blast content was obtained from 6 patients (5 patients with newly diagnosed ALL and 1 patient with relapsed ALL). Cells were isolated by Ficoll density-gradient separation. Written informed consent was obtained from all of the patients. The collection and analysis of patient samples were approved by the ethics committees of the Tokyo Medical and Dental University Institutional Review Board (approval #2010-5-2) and Hamamatsu University School of Medicine (approval #24-284).

*Animals*

Female non-obese diabetic/severe combined immunodeficient (NOD/SCID) mice were purchased from Charles River Laboratories Japan. ALL cells ($5\times10^6$ / 100 μl) infected with a lentiviral vector for *Luc2* were injected into the tail vein of NOD/SCID mice (age 6–8 week). Concentration of L-asp dose in *in vivo* experiment was decided using interview form of LEUNASE as reference. The intraperitoneal lethal dose 50 of LEUNASE in mice was estimated to be 10 U/g, therefore we performed preliminary experiments and ascertained that our mice had a tolerance to repeated intraperitoneal injection of 6 U/g L-asp and 50 mg/kg CQ administration once every day for more than 50 days. Leukemia burden was measured by luciferase activity using a luminometer (Photon Imager, Biospace Lab) after 150 mg/kg D-luciferin (Synchem UG & Co. KG)

injection. All experimental protocols conducted on the mice were approved by the Tokyo Medical and Dental University Animal Care and Use Committee.

*Measurement of intracellular and plasma amino acid levels*

Cells were washed three times with ice-cold phosphate-buffered saline (PBS) and homogenized in 80% methanol containing phenyl-d5-alanine as an internal standard for extraction, and then centrifuged (15,000 rpm for 15 minutes at 4˚C) to obtain supernatants. Samples were evaporated, and then resuspended in a small volume of water before derivatization. For amino acid analysis in plasma, mice blood samples were collected by cardiocentesis, mixed with ethylenediaminetetraacetic acid and immediately cooled on ice. Plasma was separated by centrifugation at 800 g for 15 minutes at 4˚C, and was deproteinized in a final concentration of 50% acetonitrile. The supernatant was used for the following analysis.

Amino acid analysis using high-performance liquid chromatography and electrospray ionization tandem mass spectrometry (HPLC/ESI-MS/MS) was carried out as described previously[41] with minor modifications. Samples were mixed with APDSTAG Wako Amino Acids Internal Standard Mixture Solution and derivatized with 3-aminopyridyl-N-hydroxysuccinimidyl carbamate. Derivatized samples were injected onto an Agilent 1200 series liquid chromatography system (Agilent Technologies) coupled to an API 4000 triple quadrupole mass spectrometer (Applied Biosystems-MDS Sciex). An Inertsil C8-3 column (GL Sciences Inc.) and the mobile phase A (APDSTAGTM Wako Eluent) and B (water and acetonitrile) were used for separation.

*Measurement of oxygen consumption rate (OCR) and extracellular acidification rate (ECAR)*

OCR and ECAR were measured using the Seahorse XF24 Flux Analyzer (Seahorse Bioscience). A total of $3\times10^5$ cells per well were seeded on a gelatin-coated plate in regular medium. The medium was replaced with XF Assay Medium (Seahorse Bioscience) supplemented with 1 mM pyruvate, 10 mM glucose, and 2 mM glutamine (pH 7.4) one hour before measurement. Oligomycin, carbonyl cyanide 4-(trifluoromethoxy)phenylhydrazone (FCCP), and antimycin/rotenone were added by the Flux Analyzer when indicated.

*Detection of mitochondrial membrane potential and cellular ROS*

Mitochondrial membrane potential and intracellular ROS production were measured using TMRE (tetramethylrhodamine, ethyl ester) Mitochondrial Membrane Potential Assay Kit (ab113852) and DCFDA Cellular ROS Detection Assay Kit (ab113851), respectively (both from Abcam, Cambridge, UK). For the TMRE assay, cells were incubated with 100 nM of TMRE for 15 minutes at 37 ˚C with 5 % CO2, and then suspended in PBS with 0.2 % FBS. For the ROS detection assay, cells were harvested and incubated with 10 μM of DCFDA (intracellular ROS) for 30 minutes and MitoSOX (mitochondrial ROS, Thermo Scientific) at 37 ˚C with 5% CO2. Fluorescence intensity for both procedures were measured by flow cytometry and a microplate reader.

*Cell viability assay and apoptosis assay*

ALL cells were plated at $1\times10^6$ cells in 6-well plates and treated with the appropriate reagents. Viable and dead cells were counted by trypan blue assay by the TC20 Automated Cell Counter (BioRad Laboratories). Apoptosis was assessed by flow cytometry using Annexin V/propidium iodide staining (MEBCYTO-Apoptosis Kit: MBL Co., Ltd.). All experiments were performed in triplicate.

*Cell cycle analysis*

Cells were washed in PBS, and fixed in 70% cold ethanol overnight at -20˚C. Fixed cells were washed in PBS, incubated in PBS containing RNase (250 μg/ml) for 30 minutes at 37˚C, and then stained with propidium iodide (PI, Thermo Scientific). Fluorescence intensities were measured by flow cytometry and cell population analysis was performed using the FlowJo software (Tree-star Inc.).

*Generation of L-asp-resistant cells*

L-asp–resistant cells were established by sequential incubation of parental cells with increasing concentrations of L-asp from 0.01 to 1.0 U/ml for 6 months in resistant cells from 697 cells (697-R).

*Measurement of mitochondrial DNA copy number and mitochondrial mass*

The relative ratio of mitochondrial DNA to nuclear genomic DNA was measured using the Human Mitochondrial DNA Monitoring Primer Set Ratio kit (Takara Bio). For measurement of mitochondrial mass, cells were incubated with 100 nM of MitoTracker green (Thermo Scientific) for 30 minutes, and fluorescence intensities were measured by flow cytometry.

*Immunofluorescence analysis*

Cells were fixed in cold methanol for 5 minutes. After blocking with PBS containing 1% bovine serum albumin and 0.01% Triton X-100 for 1h at 4˚C, the cells were incubated with anti-LC3B (Sigma-Aldrich) and/or human CD45-FITC antibodies (Becton, Dickinson and Company) overnight at 4˚C. Bound antibodies were visualized using Alexa Fluor 488 anti-mouse IgG antibody (Invitrogen). The cells were mounted in VECTASHIELD Mounting Medium with DAPI (Vector Laboratories). Images were obtained by confocal fluorescence microscopy (Nikon).

*Electron microscopy*

The cells were fixed with 2.5% glutaraldehyde in 0.1 M PBS overnight. They were washed with 0.1 M PBS and post-fixed with 1% $O_SO_4$ buffered in 0.1 M PBS for 2 h. Then the cells were dehydrated in a graded series of ethanol solutions and embedded in Epon 812. Ultrathin (90 nm) sections were collected on copper grids, double-stained with uranyl acetate and lead citrate, and examined by transmission electron microscopy (H-7100, Hitachi).

*Gene expression array analysis*

Gene expression profiling of ALL cells was performed as previously reported[42]. Gene ontology analysis was performed using DAVID (https://david.ncifcrf.gov/home.jsp) and gene set enrichment analysis (GSEA) (http://www.broadinstitute.org/gsea/index.jsp). The microarray data from this publication have been submitted to the GEO database (http://www.ncbi.nlm.nih.gov/geo/) and assigned the identifier GSE94289.

*Real-time polymerase chain reaction (RT-PCR)*

Quantitative real-time PCR was carried out using TaqMan polymerase with SYBR Green fluorescence (KAPA SYBR FAST qPCR Master Mix: NIPPON Genetics) on an ABI PRISM 7300 Sequence Detector (Applied Biosystems). Real-time RT-qPCR analysis was performed using specific primers (Supplementary Table S1).

*Western blotting*

Western blotting analysis was performed as previously reported[42]. Antibodies for LC3B (L7543), β-actin (A5441), and ASNS (A6485) were purchased from Sigma-Aldrich; ATF4 (L0911) was from Santa Cruz Biotechnology (Dallas, TX, USA); p53 (OP43L) was from Calbiochem (San Diego, CA, USA); cleaved PARP (#9541), cleaved CASP3 (#9661), CASP3 (#9662), CHOP (#2895), BECN1 (#4122), and ATG5 (#12994) were from Cell Signaling (Danvers, MA, USA); γH2AX (ab11174) was from Abcam.

*Transduction of short hairpin RNA (shRNA) or small interference RNA (siRNA)*

Short hairpin RNA (shRNA) oligonucleotides for *TP53* (target sequence: 5'-GACTCCAGTGGTAATCTAC-3') were annealed and inserted into the pGreenPuro vector (System Biosciences). Lentivirus was prepared using HEK293T cells and the pPACK Packaging Kit (System Biosciences) according to the manufacturer's instructions. Virus titer was measured in IFU/ml by a RT-PCR–based method using the Global UltraRapid Lentiviral Titer Kit (System Biosciences). Cells were infected with 5 MOI (multiplicity of infection; PFU/cell) of lentivirus with either an empty vector (as a control) or p53-shRNA vector using TransDux (System Biosciences).

The small interfering RNA (siRNA) for *TP53* (M-003329-03-0005), *BECN1* (M-010552-01-0005), *ATG5* (M-004374-04-0005), *ATG7* (M-020112-01-0005), and non-targeting negative control (D-001206-14-05) were obtained from Thermo Scientific Dharmacon. Cells were transfected with 10 nM of each siRNA using the HVJ Envelope Vector Kit (GENOMEONE-Neo: Ishihara Sangyo), according to the manufacturer's instructions.

*Recombinant Adenovirus infection*

The *TP53* adenovirus was prepared and cells were infected as previously described[43]. As a control, an Ad-LacZ adenovirus encoding the β-galactosidase gene was constructed from the cosmid pAxCAiLacZ (TaKaRa).

*Mutation analysis in TP53 by direct sequencing*

Mutations within coding exons in *TP53* gene were analyzed by direct DNA sequencing. DNA fragments were amplified by PCR using primer pairs described previously (http://www-p53.iarc.fr) and then PCR products were sequenced by primer for each exon.

*Statistics*

The experiments performed in ALL cell lines were performed independently in triplicate. All *P* values were 2-tailed and considered significant at $< 0.05$. Statistical analyses were performed using the statistical software EZR[44]. We analyzed drug synergism using the Chou-Talalay median-effect method[45] and used CalcuSyn software (Biosoft) to calculate the combination index (CI) and perform isobologram analysis of drug interactions.

## CONFLICT OF INTEREST

The authors declare no conflict of interest.


## ACKNOWLEDGEMENTS

We are deeply grateful to N. Hattori (Juntendo University, Japan) for use of the extracellular flux analyzer, and H. Sato, A. Hagiwara, and Y. Noguchi (Ajinomoto Co., Inc., Japan) for the intracellular amino acid analysis. We thank U. Kevin, S. Ikeda, and T Muramatsu (Tokyo Medical and Dental University, Japan) for editing of this article. We also thank R. Mori and K. Ayako (Tokyo Medical and Dental University, Japan) for technical assistance in lentivirus preparation and gene expression arrays.

Supplementary Information accompanies the paper on the Oncogene website (http://www.nature.com/onc).

## References


1 Locatelli F, Schrappe M, Bernardo ME, Rutella S. How I treat relapsed childhood acute lymphoblastic leukemia. Blood 2012; 120: 2807-2816.

2 Curran E, Stock W. How I treat acute lymphoblastic leukemia in older adolescents and young adults. Blood 2015; 125: 3702-3710.

3 Oettgen HF, Old LJ, Boyse EA, Campbell HA, Philips FS, Clarkson BD *et al*. Inhibition of leukemias in man by L-asparaginase. Cancer research 1967; 27: 2619-2631.

4 Hongo T, Yajima S, Sakurai M, Horikoshi Y, Hanada R. In vitro drug sensitivity testing can predict induction failure and early relapse of childhood acute lymphoblastic leukemia. Blood 1997; 89: 2959-2965.

5 Kaspers GJ, Veerman AJ, Pieters R, Van Zantwijk CH, Smets LA, Van Wering ER *et al*. In vitro cellular drug resistance and prognosis in newly diagnosed childhood acute lymphoblastic leukemia. Blood 1997; 90: 2723-2729.

6 Aslanian AM, Kilberg MS. Multiple adaptive mechanisms affect asparagine synthetase substrate availability in asparaginase-resistant MOLT-4 human leukaemia cells. Biochem J 2001; 358: 59-67.

7 Stams WA, den Boer ML, Holleman A, Appel IM, Beverloo HB, van Wering ER *et al*. Asparagine synthetase expression is linked with L-asparaginase resistance in TEL-AML1-negative but not TEL-AML1-positive pediatric acute lymphoblastic leukemia. Blood 2005; 105: 4223-4225.

8 Su N, Pan YX, Zhou M, Harvey RC, Hunger SP, Kilberg MS. Correlation between asparaginase sensitivity and asparagine synthetase protein content, but not mRNA, in acute lymphoblastic leukemia cell lines. Pediatric blood & cancer 2008; 50: 274-279.

9 Stams WA, den Boer ML, Beverloo HB, Meijerink JP, Stigter RL, van Wering ER *et al*. Sensitivity to L-asparaginase is not associated with expression levels of asparagine synthetase in t(12;21)+ pediatric ALL. Blood 2003; 101: 2743-2747.

10 Holleman A, Cheok MH, den Boer ML, Yang W, Veerman AJ, Kazemier KM *et al*. Gene-expression patterns in drug-resistant acute lymphoblastic leukemia cells and response to treatment. The New England journal of medicine 2004; 351: 533-542.

11 Fine BM, Kaspers GJ, Ho M, Loonen AH, Boxer LM. A genome-wide view of the in vitro response to l-asparaginase in acute lymphoblastic leukemia. Cancer research 2005; 65: 291-299.

12 Hermanova I, Zaliova M, Trka J, Starkova J. Low expression of asparagine synthetase in lymphoid blasts precludes its role in sensitivity to L-asparaginase. Exp Hematol 2012; 40: 657-665.

13 Choi AM, Ryter SW, Levine B. Autophagy in human health and disease. The New England journal of medicine 2013; 368: 651-662.

14 Amaravadi RK, Lippincott-Schwartz J, Yin XM, Weiss WA, Takebe N, Timmer W *et al*. Principles and current strategies for targeting autophagy for cancer treatment. Clin Cancer Res 2011; 17: 654-666.

15 Rebecca VW, Amaravadi RK. Emerging strategies to effectively target autophagy in cancer. Oncogene 2016; 35: 1-11.

16 Yu M, Henning R, Walker A, Kim G, Perroy A, Alessandro R *et al*. L-asparaginase inhibits invasive and angiogenic activity and induces autophagy in ovarian cancer. Journal of cellular and molecular medicine 2012; 16: 2369-2378.

17 Hermanova I, Arruabarrena-Aristorena A, Valis K, Nuskova H, Alberich-Jorda M, Fiser K *et al*. Pharmacological inhibition of fatty-acid oxidation synergistically enhances the effect of l-asparaginase in childhood ALL cells. Leukemia 2015.

18 Song P, Ye L, Fan J, Li Y, Zeng X, Wang Z *et al*. Asparaginase induces apoptosis and cytoprotective autophagy in chronic myeloid leukemia cells. Oncotarget 2015; 6: 3861-3873.

19 Sherman BT, Huang da W, Tan Q, Guo Y, Bour S, Liu D *et al*. DAVID Knowledgebase: a gene-centered database integrating heterogeneous gene annotation resources to facilitate high-throughput gene functional analysis. BMC bioinformatics 2007; 8: 426.

20 Subramanian A, Tamayo P, Mootha VK, Mukherjee S, Ebert BL, Gillette MA *et al*. Gene set enrichment analysis: a knowledge-based approach for interpreting genome-wide expression profiles. Proc Natl Acad Sci U S A 2005; 102: 15545-15550.

21 Klionsky DJ, Abdalla FC, Abeliovich H, Abraham RT, Acevedo-Arozena A, Adeli K *et al*. Guidelines for the use and interpretation of assays for monitoring autophagy. Autophagy 2012; 8: 445-544.

22 Ueno T, Ohtawa K, Mitsui K, Kodera Y, Hiroto M, Matsushima A *et al*. Cell cycle arrest and apoptosis of leukemia cells induced by L-asparaginase. Leukemia 1997; 11: 1858-1861.

23 Reddy PN, Sargin B, Choudhary C, Stein S, Grez M, Muller-Tidow C *et al*. SOCS1 cooperates with FLT3-ITD in the development of myeloproliferative disease by promoting the escape from external cytokine control. Blood 2012; 120: 1691-1702.

24 Velasco-Hernandez T, Hyrenius-Wittsten A, Rehn M, Bryder D, Cammenga J. HIF-1alpha can act as a tumor suppressor gene in murine acute myeloid leukemia. Blood 2014; 124: 3597-3607.

25 Ye J, Kumanova M, Hart LS, Sloane K, Zhang H, De Panis DN *et al*. The GCN2-ATF4 pathway is critical for tumour cell survival and proliferation in response to nutrient deprivation. The EMBO journal 2010; 29: 2082-2096.

26 Sablina AA, Budanov AV, Ilyinskaya GV, Agapova LS, Kravchenko JE, Chumakov PM. The antioxidant function of the p53 tumor suppressor. Nature medicine 2005; 11: 1306-1313.

27 Ranjan A, Iwakuma T. Non-Canonical Cell Death Induced by p53. International journal of molecular sciences 2016; 17.

28 Amaravadi RK, Yu D, Lum JJ, Bui T, Christophorou MA, Evan GI *et al*. Autophagy inhibition enhances therapy-induced apoptosis in a Myc-induced model of lymphoma. The Journal of clinical investigation 2007; 117: 326-336.

29 Degenhardt K, Mathew R, Beaudoin B, Bray K, Anderson D, Chen G *et al*. Autophagy promotes tumor cell survival and restricts necrosis, inflammation, and tumorigenesis. Cancer cell 2006; 10: 51-64.

30 Maiuri MC, Zalckvar E, Kimchi A, Kroemer G. Self-eating and self-killing: crosstalk between autophagy and apoptosis. Nature reviews Molecular cell biology 2007; 8: 741-752.

31 Lorenzi PL, Claerhout S, Mills GB, Weinstein JN. A curated census of autophagy-modulating proteins and small molecules: candidate targets for cancer therapy. Autophagy 2014; 10: 1316-1326.

32 Bonapace L, Bornhauser BC, Schmitz M, Cario G, Ziegler U, Niggli FK *et al*. Induction of autophagy-dependent necroptosis is required for childhood acute lymphoblastic leukemia cells to overcome glucocorticoid resistance. The Journal of clinical investigation 2010; 120: 1310-1323.

33 Laane E, Tamm KP, Buentke E, Ito K, Kharaziha P, Oscarsson J *et al*. Cell death induced by dexamethasone in lymphoid leukemia is mediated through initiation of autophagy. Cell death and differentiation 2009; 16: 1018-1029.

34 Polak A, Kiliszek P, Sewastianik T, Szydlowski M, Jablonska E, Bialopiotrowicz E *et al*. MEK Inhibition Sensitizes Precursor B-Cell Acute Lymphoblastic Leukemia (B-ALL) Cells to Dexamethasone through Modulation of mTOR Activity and Stimulation of Autophagy. PLoS One 2016; 11: e0155893.

35 Bush A, Cunningham S, de Blic J, Barbato A, Clement A, Epaud R *et al*. European protocols for the diagnosis and initial treatment of interstitial lung disease in children. Thorax 2015.

36 Barrera V, Hiscott PS, Craig AG, White VA, Milner DA, Beare NA *et al*. Severity of retinopathy parallels the degree of parasite sequestration in the eyes and brains of malawian children with fatal cerebral malaria. J Infect Dis 2015; 211: 1977-1986.

37 Eng CH, Wang Z, Tkach D, Toral-Barza L, Ugwonali S, Liu S *et al*. Macroautophagy is dispensable for growth of KRAS mutant tumors and chloroquine efficacy. Proc Natl Acad Sci U S A 2016; 113: 182-187.

38 Rosenfeldt MT, O'Prey J, Morton JP, Nixon C, MacKay G, Mrowinska A *et al*. p53 status determines the role of autophagy in pancreatic tumour development. Nature 2013; 504: 296-300.

39 Lee SW, Kim HK, Lee NH, Yi HY, Kim HS, Hong SH *et al*. The synergistic effect of combination temozolomide and chloroquine treatment is dependent on autophagy formation and p53 status in glioma cells. Cancer Lett 2015; 360: 195-204.

40 Stengel A, Schnittger S, Weissmann S, Kuznia S, Kern W, Kohlmann A *et al*. TP53 mutations occur in 15.7% of ALL and are associated with MYC-rearrangement, low hypodiploidy, and a poor prognosis. Blood 2014; 124: 251-258.

41 Shimbo K, Oonuki T, Yahashi A, Hirayama K, Miyano H. Precolumn derivatization reagents for high-speed analysis of amines and amino acids in biological fluid using liquid chromatography/electrospray ionization tandem mass spectrometry. Rapid Commun Mass Spectrom 2009; 23: 1483-1492.

42 Fujiwara N, Inoue J, Kawano T, Tanimoto K, Kozaki K, Inazawa J. miR-634 Activates the Mitochondrial Apoptosis Pathway and Enhances Chemotherapy-Induced Cytotoxicity. Cancer research 2015; 75: 3890-3901.

43 Inoue J, Misawa A, Tanaka Y, Ichinose S, Sugino Y, Hosoi H *et al*. Lysosomal-associated protein multispanning transmembrane 5 gene (LAPTM5) is associated with spontaneous regression of neuroblastomas. PLoS One 2009; 4: e7099.

44 Kanda Y. Investigation of the freely available easy-to-use software 'EZR' for medical statistics. Bone Marrow Transplant 2013; 48: 452-458.

45 Chou TC. Drug combination studies and their synergy quantification using the Chou-Talalay method. Cancer research 2010; 70: 440-446.

## FIGURE LEGENDS

**Figure 1. Induction of metabolic shutdown by L-asparaginase treatment**

**a.** Intracellular analysis of asparagine, glutamine, and ATP. REH cells were treated with 1 U/ml of L-asp for the indicated time. Data are represented as relative ratio to control at each incubation time.

**b.** Expression array analysis in L-asp–treated REH cells. REH cells were treated with 1 U/ml of L-asp for 48 hours. GO terms associated with metabolism from DAVID analysis. All candidate GO terms are ranked by *P*-value, and are listed in Supplementary Table S2. Bars indicate the counts of genes included in the respective gene set for each GO term. Line indicates *P* values in $\log_{10}$.

**c.** GSEA of microarray expression data comparing untreated and L-asp–treated REH cells. NES, normal enrichment score.

**d.** Quantitative RT-PCR analysis for glycolysis-, TCA cycle-, and OXPHOS-related genes in L-asp–treated REH cells (1 U/ml of L-asp for 48 h). Expression of *β-actin* was used as an internal control. Expression levels relative to those in the untreated cells are indicated on the vertical axis. *P* values were calculated using two-sided Student's t-test (*$p < 0.05$, **$p < 0.01$).

**e.** Absolute OCR and ECAR values of untreated and L-asp–treated REH cells (1 U/ml of L-asp for 48 h).

**f.** Mitochondria stress test in untreated and L-asp–treated cells. OCR levels were calculated by normalization to cell number.

**Figure 2. Induction of autophagy by L-asparaginase treatment**

**a.** Western blot analysis of REH and 697 cells. Fold change of LC3B-II level (normalized to β-actin) relative to that of untreated cells is indicated in the graph in the lower panel.

**b.** Immunofluorescence analysis of LC3B protein. Square areas are enlarged and shown in the lower panel. Scale bars represent 10 μm.

**c.** Representative images of electron microscopic analysis. Arrow and arrowhead indicate an autolysosome and autophagosome, respectively. Numbers and areas of these autophagic vacuoles per cell were analyzed using ImageJ. Fifty cells were investigated per group. Scale bars represent 500 nm. Data represent as mean ± SD.

**d.** Mitochondrial membrane potential assay with TMRE. Fluorescence intensity was measured using flow cytometry.

**e.** Measurement of intracellular and mitochondrial ROS level. Treated REH cells were stained with 10 μM of DCFDA (intracellular ROS) or 2.5 μM of MitoSox (mitochondrial ROS).

REH cells were treated with 1 U/ml of L-asp for 48 h and/or 10 μM of CQ for the last 3 h (**a**–**d**) or for 48 h (**d** and **e**). Data in **a**, **c–e** represent as mean ± SD ($n = 3$); $^{*}P < 0.05$, $^{***}P < 0.001$. *P* values were calculated using one-way ANOVA.

**Figure. 3. Effect of autophagy inhibition on L-asparaginase-induced cytotoxicity in ALL cells.**

**a and b.** Apoptotic analysis in ALL cell lines REH and 697 cells with or without CQ-treatment by flow cytometry (**a**) and western blotting (**b**). The proportion of dead cells was measured by flow cytometry using Annexin-V staining. Cells were treated with the indicated concentrations of L-asp and/or CQ for 48 h.

**c.** Cell survival assay during prolonged treatment. According to the clinical method for administering L-asp which is repeated every 3 days in patients, ALL cells were cultured with PBS (control) or repeated (0, 72, 144 h) administration of L-asp and/or CQ. Viable cells were counted using trypan blue staining every 24 h. ALL cells were treated with repeated administration of L-asp and/or CQ.

**d.** Sensitivity to L-asp treatment in REH cells transfected with *ATG7*-siRNA. Cells transfected with control-siRNA (si-control) or *ATG7*-siRNA (si-ATG7) were treated with the indicated concentrations of L-asp for 48 h. Viable cells were counted by flow cytometry using Annexin-V staining.

**e.** Cell survival assay of parental cells and L-asp–resistant cells generated from 697 cells (697-R).

**f.** Apoptotic analysis of 697-R cells.

**g.** Western blot analysis of parental cells and 697-R cells.

Data in **a** and **d**–**f** are represented as mean ± SD (n = 3; *p < 0.05, **p < 0.01, ***p < 0.001). P values were calculated using two-sided Student's t-test (**a** and **f**), and one-way ANOVA (**c**).

**Figure. 4. Therapeutic potential of autophagy inhibition upon treatment with L-asparaginase in ALL xenograft model.**

**a.** Quantification of bioluminescent signals in mice transplanted with luciferase-transduced REH cells at day 7 after transplantation. The graph indicates no significant difference was observed among the four treatment groups (control, *n*=7; CQ, *n*=9; L-asp, *n*=8; L-asp+CQ, *n*=11) in photon flux.

**b.** Measurement of peripheral amino acid levels by LC-MS/MS. Samples were prepared from the plasma of mice at day 14 after administration in independent experiments. The levels were normalized to the volume of drawn blood. Data represent as mean ± SD (*n* = 3).

**c.** Whole-body mouse imaging. A pseudocolor scale shows relative bioluminescence changes over time.

**d.** Kaplan-Meier overall survival curve in mice treated with PBS only (control, *n*=7), CQ (50 mg/kg, *n*=9), L-asp (6 U/g, *n*=8), or L-asp plus CQ (6 U/g and 50 mg/kg, respectively, *n*=11).

**e.** Body weight at day 22 after transplantation (control, *n*=7; CQ, *n*=9; L-asp, *n*=8; L-asp+CQ, *n*=11).

**f.** Liver weight (% body weight) of control or treated mice. Mice were sacrificed at day 15 after transplantation (n=*5* per group).

P-values were calculated using one-way ANOVA (**a**, **b**, **e**, and **f**) and log-rank test (**d**) (*p < 0.05, ***p < 0.001; ND, not detected; NS, not significant).

**Figure 5. Activation of the ROS-p53 feedback loop by combination treatment of L-asparaginase and chloroquine in ALL cells.**

**a.** Effect of NAC on induction of cell death. REH cells were concurrently treated with 2mM of NAC with 1 U/ml of L-asp and/or 10 μM of CQ for 48 h.

**b.** Western blot analysis of L-asp and/or CQ-treated REH cells.

**c.** Western blot analysis of NAC-treated REH cells. L-asp and/or CQ-treated cells were concurrently treated with 2mM NAC for 48 h.

**d**–**f.** Cellular ROS detection assay (**d**), Western blot analysis (**e**), and apoptosis analysis (**f**) of *TP53*-knockdown REH cells.

**g.** Kaplan-Meier overall survival curve in mice. NOD/SCID mice were transplanted with REH-Luc2 cells

stably transfected with sh-control or sh-p53 by tail vein injection. These mice were treated as described in Figure 4d ($n$=5 per group).

**h.** Cell survival assay in primary ALL samples. ALL cells were purified from the bone marrow of samples from ALL patients shown in Supplementary Table S3. Cells were treated with 1 U/ml of L-asp and/or 10 μM of CQ for 48 h, and viable cells were measured by flow cytometry using Annexin-V staining.

**i.** Effect of p53 expression on cell survival in ALL cells purified from patient No.7. Cells transduced with Ad-LacZ (as a control) or Ad-p53 were treated with 1 U/ml of L-asp and/or 10 μM of CQ for 48 h. Viable cells were measured as described in **h**.

Data in **a**, **d**, **f**, **h**, and **i** represent as mean ± SD ($n$ = 3); $^{*}P < 0.05$, $^{**}P < 0.01$, $^{***}P < 0.001$; NS, not significant. P values were calculated using two-sided Student's t-test (**a**, **d**, **f**, **h**, and **i**), and log-rank test (**g**).

**Figure 6. Schematic diagram.**

L-asparaginase treatment induces mitochondrial injury. Autophagy contributes to the prevention of oxidative DNA damage accumulation in L-asparaginase–treated cells. Autophagy inhibition with L-asp treatment triggers the ROS-DNA damage-p53 feedback loop, which leads to marked apoptosis in ALL cells.

# Figure 1

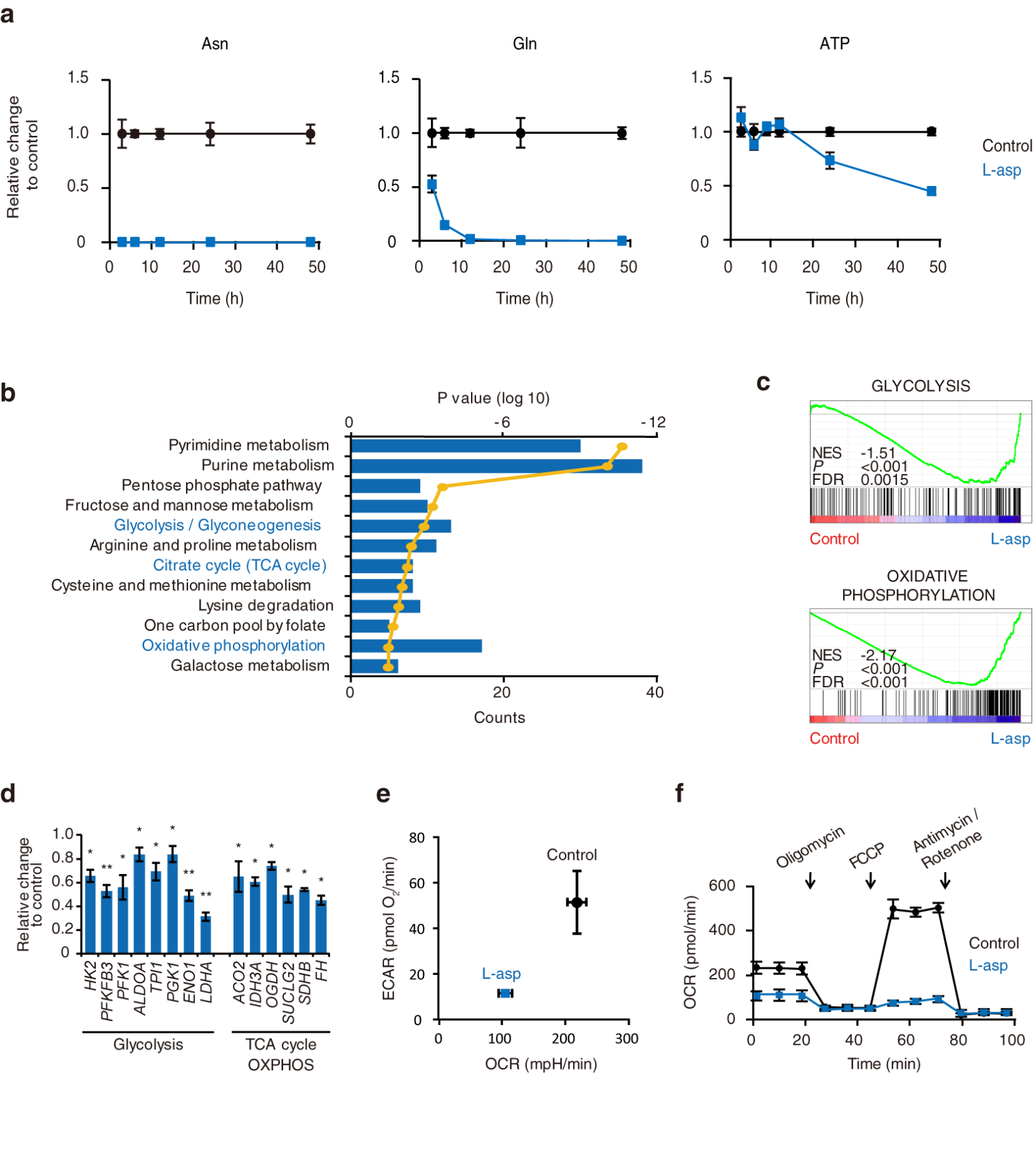
a
Asn
Gln
ATP
Relative change to control
1.5
1.0
0.5
0
0 10 20 30 40 50
Time (h)
Control
L-asp
b
P value (log 10)
0
-6
-12
Pyrimidine metabolism
Purine metabolism
Pentose phosphate pathway
Fructose and mannose metabolism
Glycolysis / Glyconeogenesis
Arginine and proline metabolism
Citrate cycle (TCA cycle)
Cysteine and methionine metabolism
Lysine degradation
One carbon pool by folate
Oxidative phosphorylation
Galactose metabolism
0 20 40
Counts
c
GLYCOLYSIS
NES -1.51
P <0.001
FDR 0.0015
Control
L-asp
OXIDATIVE PHOSPHORYLATION
NES -2.17
P <0.001
FDR <0.001
Control
L-asp
d
Relative change to control
1.0
0.8
0.6
0.4
0.2
0
HK2
PFKFB3
PFK1
ALDOA
TPI1
PGK1
ENO1
LDHA
ACO2
IDH3A
OGDH
SUCLG2
SDHB
FH
Glycolysis
TCA cycle
OXPHOS
e
ECAR (pmol O2/min)
80
60
40
20
0
Control
L-asp
0 100 200 300
OCR (mpH/min)
f
Oligomycin
FCCP
Antimycin / Rotenone
OCR (pmol/min)
600
400
200
0
Control
L-asp
0 20 40 60 80 100
Time (min)

# Figure 2

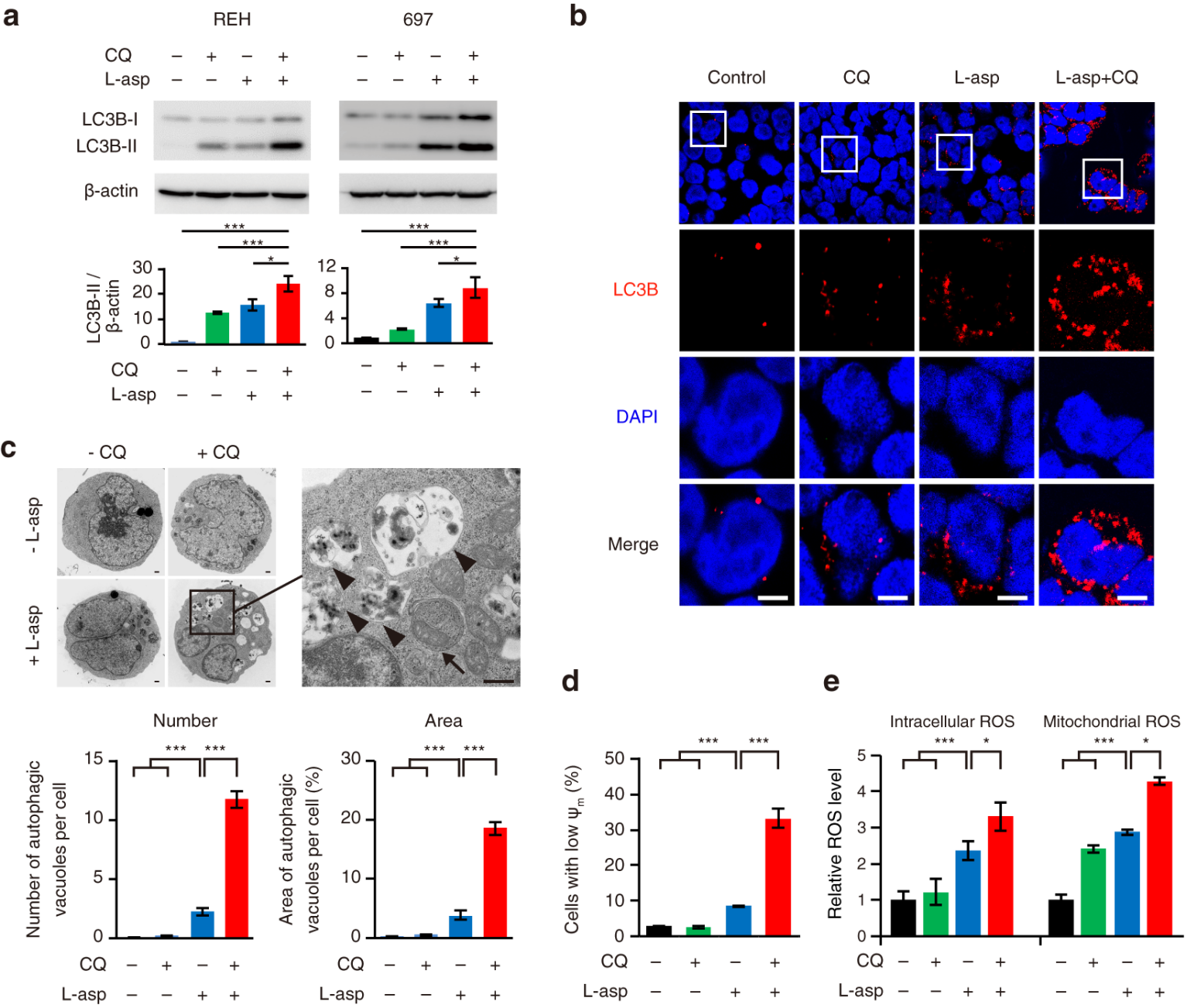
a
REH
697
CQ
L-asp
LC3B-I
LC3B-II
β-actin
LC3B-II / β-actin
b
Control
CQ
L-asp
L-asp+CQ
LC3B
DAPI
Merge
c
- CQ
+ CQ
- L-asp
+ L-asp
Number
Area
Number of autophagic vacuoles per cell
Area of autophagic vacuoles per cell (%)
d
Cells with low ψm (%)
e
Intracellular ROS
Mitochondrial ROS
Relative ROS level

# Figure 3

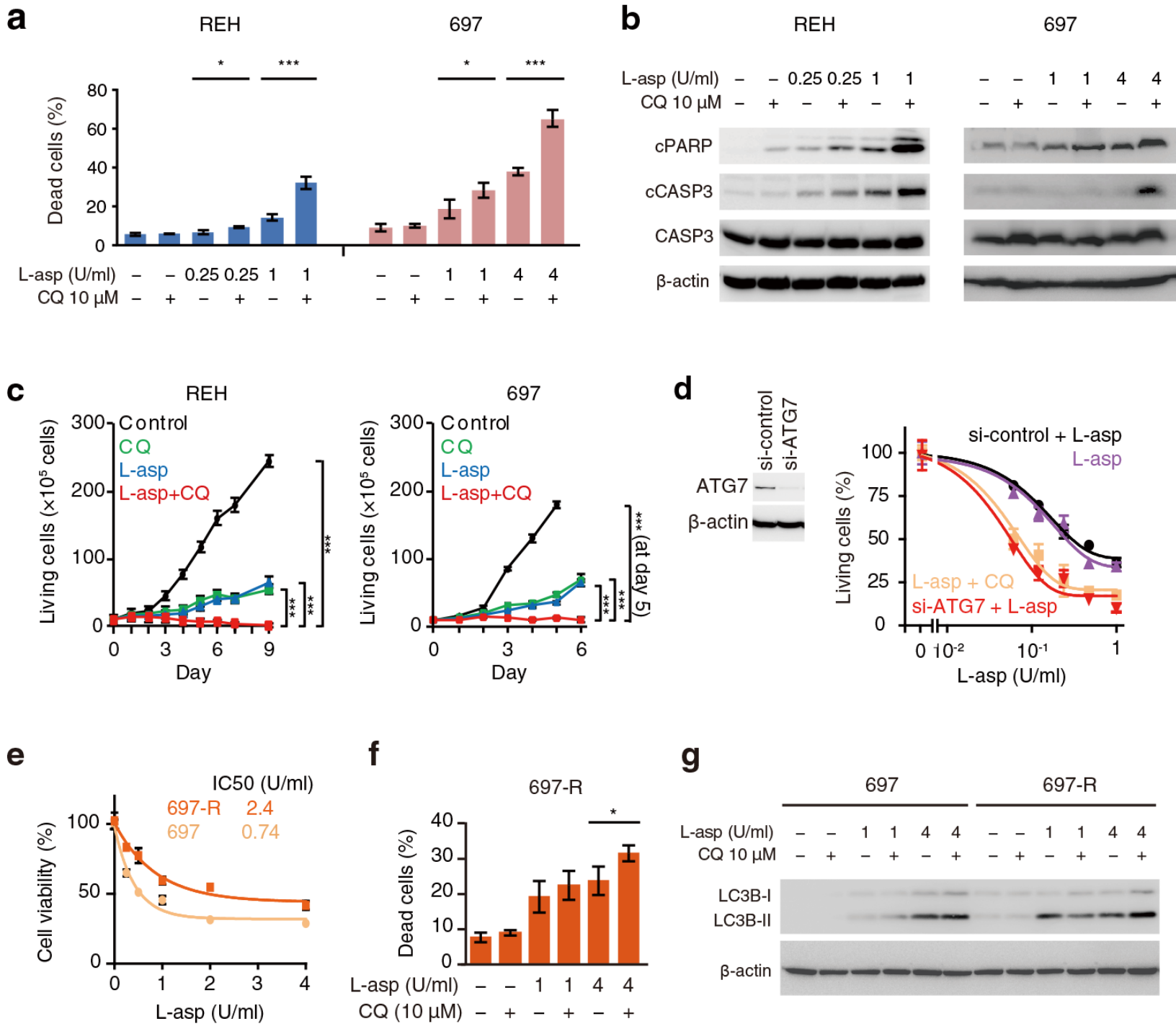
a
REH
697
Dead cells (%)
L-asp (U/ml)
CQ 10 μM
b
REH
697
L-asp (U/ml)
CQ 10 μM
cPARP
cCASP3
CASP3
β-actin
c
REH
697
Control
CQ
L-asp
L-asp+CQ
Living cells (×10⁵ cells)
Day
(at day 5)
d
si-control
si-ATG7
ATG7
β-actin
si-control + L-asp
L-asp
L-asp + CQ
si-ATG7 + L-asp
Living cells (%)
L-asp (U/ml)
e
IC50 (U/ml)
697-R 2.4
697 0.74
Cell viability (%)
L-asp (U/ml)
f
697-R
Dead cells (%)
L-asp (U/ml)
CQ (10 μM)
g
697
697-R
L-asp (U/ml)
CQ 10 μM
LC3B-I
LC3B-II
β-actin

# Figure 4

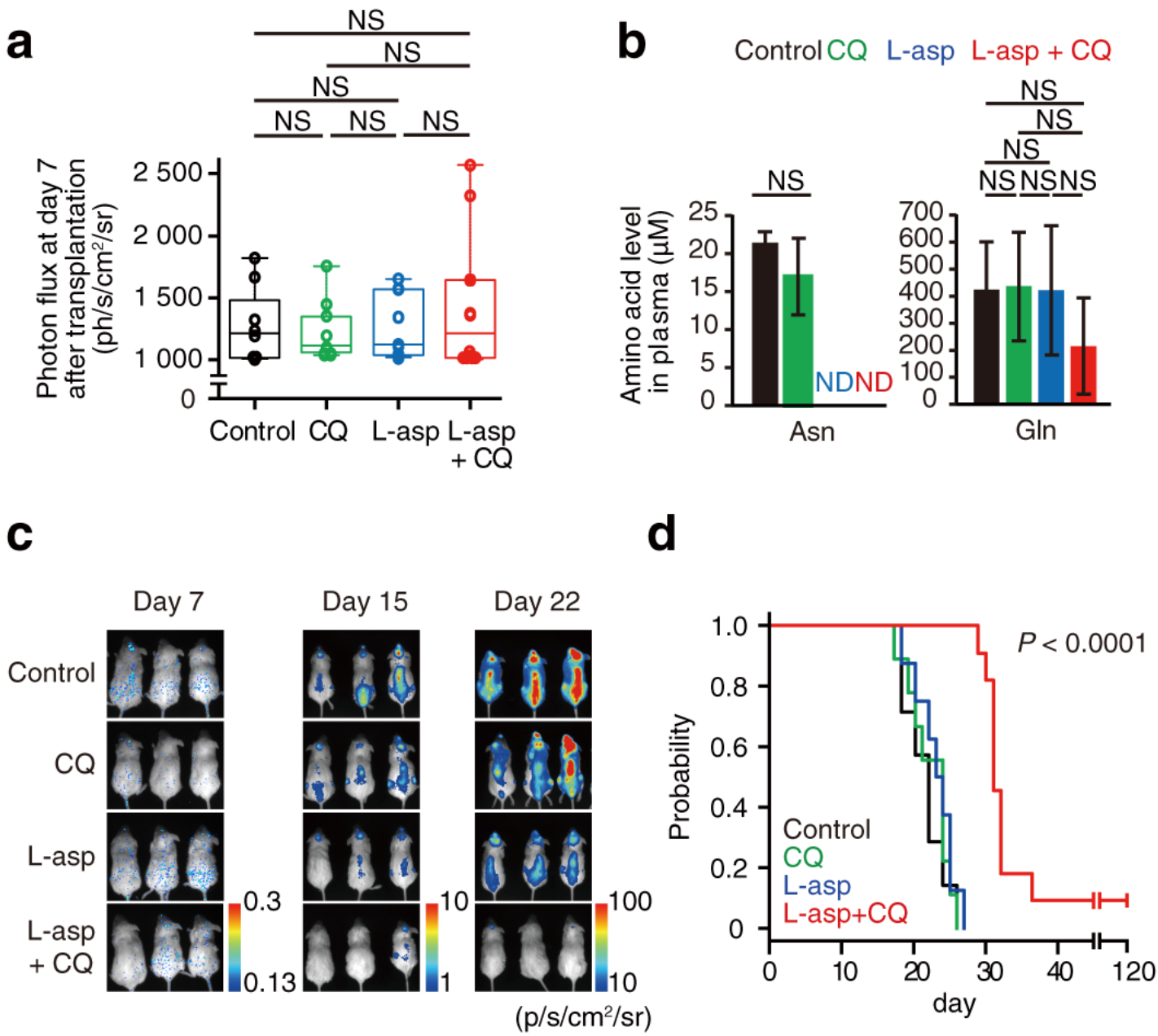
a
NS
NS
NS
NS NS NS
Photon flux at day 7 after transplantation (ph/s/cm²/sr)
2 500
2 000
1 500
1 000
0
Control CQ L-asp L-asp + CQ
b
Control CQ L-asp L-asp + CQ
NS
NS
NS
NS NS NS
Amino acid level in plasma (μM)
25
20
15
10
5
0
ND ND
Asn
700
600
500
400
300
200
100
0
Gln
c
Day 7
Day 15
Day 22
Control
CQ
L-asp
L-asp + CQ
0.3
0.13
10
1
100
10
(p/s/cm²/sr)
d
P < 0.0001
Probability
1.0
0.8
0.6
0.4
0.2
0
Control
CQ
L-asp
L-asp+CQ
0 10 20 30 40 120
day
e
*
*
***
Body weight at Day 22 (g)
20
18
16
14
12
10
8
0
Control CQ L-asp L-asp + CQ
f
***
***
*
Liver weight at Day 15 (% dody weight)
7
6
5
4
3
0
Control CQ L-asp L-asp + CQ

# Figure 5

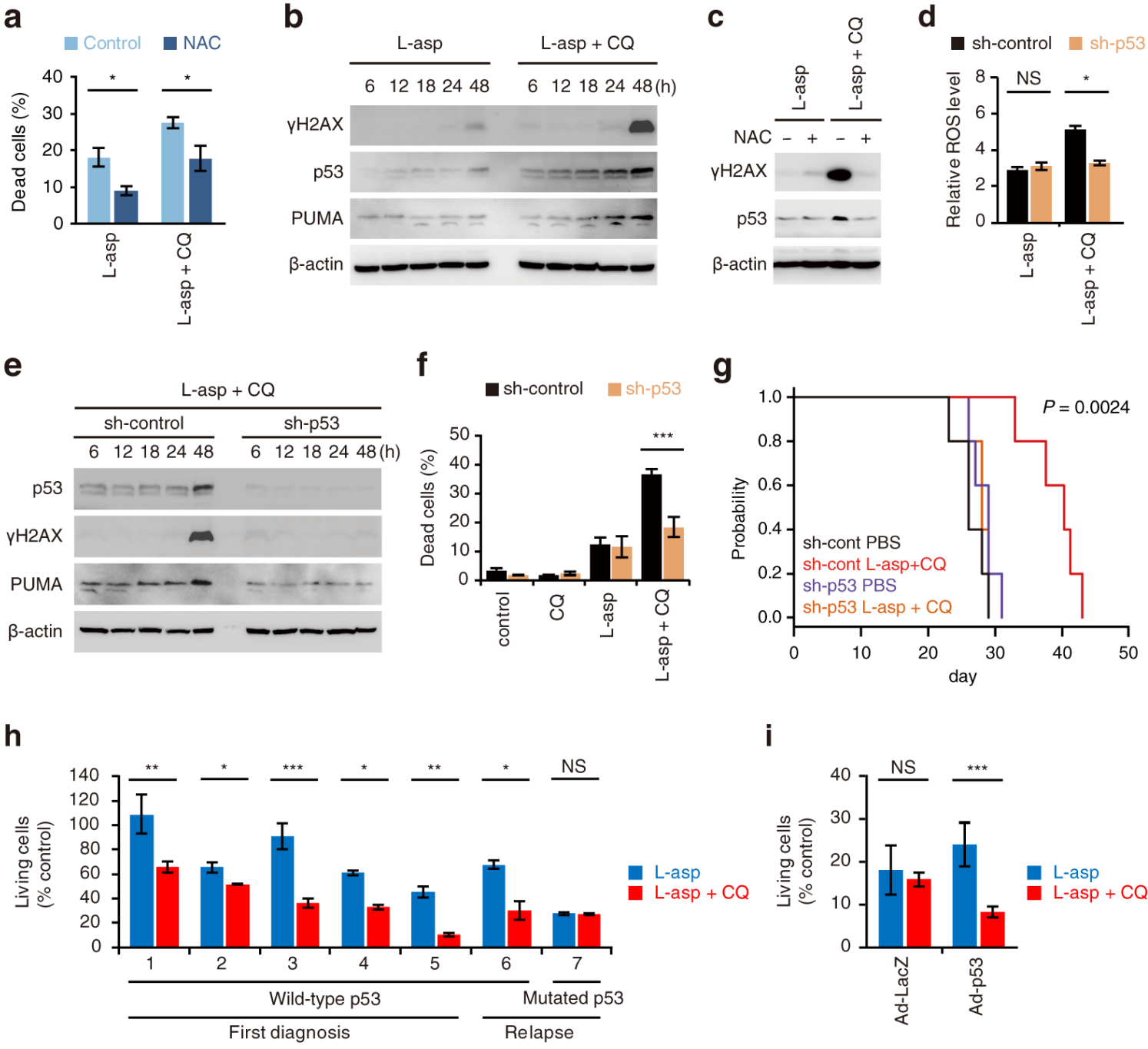
a
Control
NAC
Dead cells (%)
40
30
20
10
0
*
*
L-asp
L-asp + CQ
b
L-asp
L-asp + CQ
6 12 18 24 48
6 12 18 24 48 (h)
γH2AX
p53
PUMA
β-actin
c
L-asp
L-asp + CQ
NAC – + – +
γH2AX
p53
β-actin
d
sh-control
sh-p53
Relative ROS level
8
6
4
2
0
NS
*
L-asp
L-asp + CQ
e
L-asp + CQ
sh-control
sh-p53
6 12 18 24 48
6 12 18 24 48 (h)
p53
γH2AX
PUMA
β-actin
f
sh-control
sh-p53
Dead cells (%)
50
40
30
20
10
0
***
control
CQ
L-asp
L-asp + CQ
g
P = 0.0024
Probability
1.0
0.8
0.6
0.4
0.2
0.0
sh-cont PBS
sh-cont L-asp+CQ
sh-p53 PBS
sh-p53 L-asp + CQ
0
10
20
30
40
50
day
h
Living cells (% control)
140
120
100
80
60
40
20
0
**
*
***
*
**
*
NS
1
2
3
4
5
6
7
Wild-type p53
Mutated p53
First diagnosis
Relapse
L-asp
L-asp + CQ
i
Living cells (% control)
40
30
20
10
0
NS
***
Ad-LacZ
Ad-p53
L-asp
L-asp + CQ

**Figure 6**

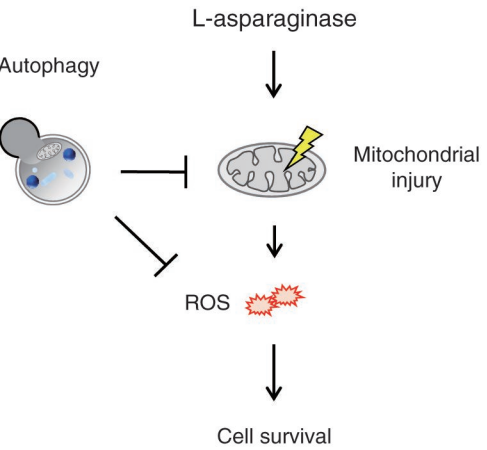
L-asparaginase
Autophagy
Mitochondrial injury
ROS
Cell survival

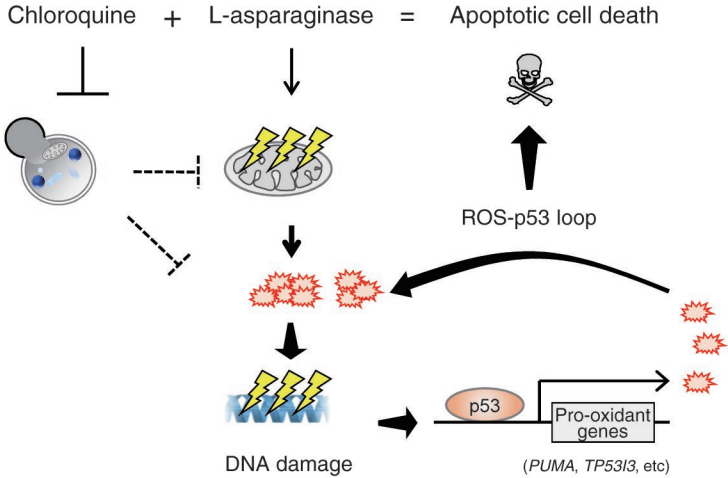
Chloroquine
+
L-asparaginase
=
Apoptotic cell death
ROS-p53 loop
DNA damage
p53
Pro-oxidant genes
(PUMA, TP53I3, etc)